

DIRECT (UNDER) SAMPLING VS. ANALOG DOWNCONVERSION FOR BPM ELECTRONICS*

M. Wendt[#], CERN, Geneva, Switzerland

Abstract

Digital signal processing by means of undersampling the analog signal has become a popular method for acquiring beam position monitor signals. This presentation discusses the technique and its principle limitations, presents today's technical limits (e.g. in terms of performance of available ADCs), and provides an outlook for the future. It will also try to compare the technique with more tradition analog downmixing and signal processing methods

INTRODUCTION

Beam position monitors (BPM) are the workhorse of the beam diagnostics for every particle accelerator, linear, circular or transport lines, operating with leptons, hadrons or ions. A system of many, synchronized BPMs, distributed along the accelerator's beam-line allows the observation of the beam orbit, and, using well adapted read-out electronics, enables the extraction of a manifold of relevant information of the performance of the accelerator and it's beam quality. It is the optimization of BPM pickup, read-out electronics and data acquisition system, matched to the properties of accelerator and beam, which defines performance, quality and reproducibility of this important beam instrumentation system.

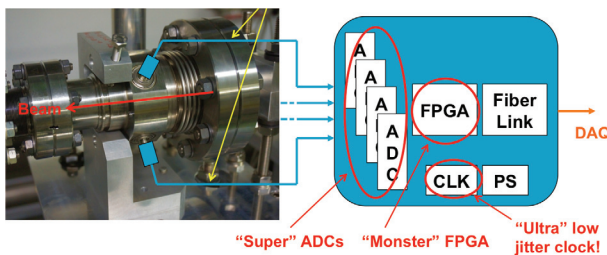


Figure 1: The ultimate digital BPM read-out electronics?

While the combination of both, the BPM pickup and the read-out electronics defines the ultimate performance in terms of resolution and long-term stability, most of the progress on these parameters have been made in recent years due to improvements in the read-out electronics, namely by adapting digital technologies, with profits taken from the commercial and military chip developments. Fig. 1 illustrates a provocative, "all digital" BPM electronics, using "super" ADCs and other equivalent components, hooked directly to the pickup electrodes.

Even with todays most advanced semiconductors, this idea is not feasible. Analog and RF components are still

required in the signal path to guarantee the expected BPM performance, and to keep the costs reasonable, as the accelerator has to be equipped with many, sometimes more than 1000 beam position monitors, e.g. the LHC [1].

This work focuses on aspects of present technologies for BPM read-out electronics, trying to evaluate how much analog RF electronics is still necessary, and what can and should be accomplished digitally. A more general summary on trends and developments for BPM systems has been published some years ago [2].

BEAM SIGNALS

Understanding the beam properties, and the signals and characteristics of the BPM pickup is mandatory to specify and develop the optimal, best-suited read-out electronics.

Broadband BPM Pickups

A typical broadband BPM pickup consists out of symmetrically arranged RF antennas, typically "button" or stripline-like electrodes, which interact to the electromagnetic field of the passing beam.

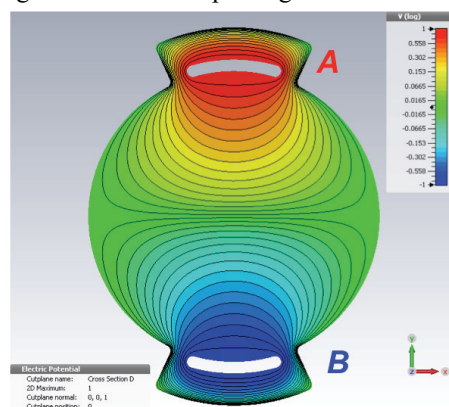


Figure 2: Equipotentials of a stripline BPM.

Figure 2 shows the cross-section of a stripline BPM with symmetrically arranged electrodes, for simplicity only the vertical ones. Plotted are the equipotentials for a potential difference between the electrodes, which indicate contour lines of beam positions giving constant signal amplitudes A and B. The beam displacement, or beam position is measured by detecting the asymmetry of these amplitudes, and normalizing them such that the beam position measurement is independent from the absolute signal level, as this varies with the beam intensity:

$$\text{norm. beam position} \propto \frac{A - B}{A + B}. \quad (1)$$

The output signal of a BPM electrode or pickup is given by

$$V_{elec}(x, y, \omega) = s(x, y) Z(\omega) I_{beam}(\omega) \quad (2)$$

where $Z(\omega)$ is the frequency dependent transfer impedance of the BPM electrode, and $s(x, y)$ is a sensitivity function which reflects the geometry of the beam pickup, thus the position characteristic. For broadband BPM pickups $s(x, y)$ is frequency independent, but nor for resonant BPMs.

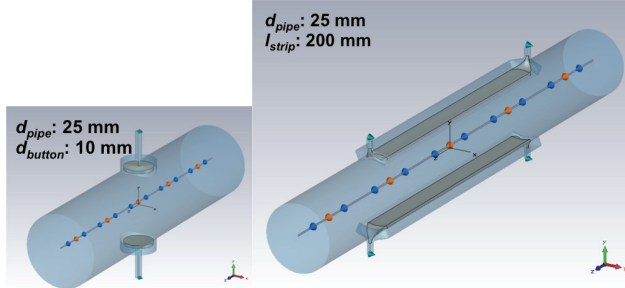


Figure 3: “Button” (left) and stripline (right) BPM pickups.

The transfer impedance $Z(\omega)$ of a BPM electrode can be estimated analytically, e.g. for a “button” electrode:

$$Z_{button}(\omega) = \phi R_{load} \left(\frac{\omega_1}{\omega_2} \right) \frac{(\omega_1 / \omega_2)}{1 + (\omega_1 / \omega_2)^2} \quad (2)$$

with: $\omega_1 = \frac{1}{R_{load} C_{button}}$, $\omega_2 = \frac{c_0}{2 r_{button}}$, $\phi = \frac{r_{button}}{4 r_{pipe}}$

and for a stripline electrode:

$$Z_{strip}(\omega) = i \phi Z_0 e^{-i \frac{\omega l_{strip}}{c_0}} \sin \left(\frac{\omega l_{strip}}{c_0} \right) \quad (2)$$

However, a quick numerical analysis, e.g. here accomplished by using the *CST Studio Suite* wakefield solver, will give directly output signal of the BPM electrode for a specific beam condition. Figure 3 shows the geometries of the analysed button and stripline BPMs. The simulated beam bunch was *Gaussian*, with $n=10^{10}$ electrons, $\sigma=25$ mm, travelling at $v=c_0$ on an orbit with a vertical offset ($x=0, y=+1$ mm).

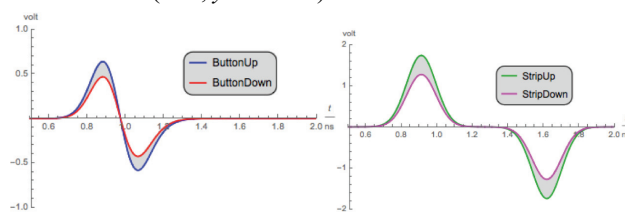


Figure 4: Time domain output signals of the button (left) and stripline (right) BPM electrodes for a single bunch passing with a +1mm vertical beam offset.

Figure 4 shows the time domain output signals from both, button and stripline electrodes. As of the vertical beam offset, the signal amplitude of the upper electrode is larger for both pickup styles. However, the shape of the signal waveform is different, also the amplitudes of the stripline BPM electrodes are higher. In both cases, the single bunch response is a short, differentiated pulse waveform in the nano-second regime, i.e. for most of the

time there is no signal (“0” volt) if bunches are spaced far.

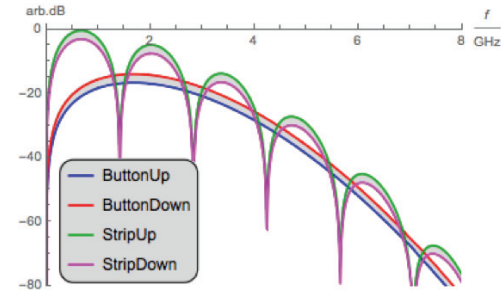


Figure 5: Frequency domain representation of the signals of Fig. 4, scaled to arbitrary dB.

Figure 5 shows the frequency domain representation of the signals of Fig. 4, scaled to dB. Noticeable, for both BPM styles the amplitude difference between the output signals of the electrodes is ~2.7 dB, and is constant over the entire output frequency spectrum. The stripline BPM outputs higher signal levels, particular at lower frequencies, e.g. at 500 MHz the stripline signal level is ~20 dB higher compared to the button electrode.

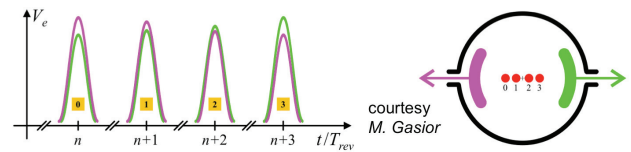


Figure 6: Turn-by-turn beam oscillations at the BPM.

Figure 6 illustrates the amplitude modulation of the BPM electrode signals due to the transverse bunched beam oscillations on a turn-by-turn basis. Both BPM electrodes deliver a high, common-mode signal, defined by the beam intensity, amplitude modulated by a small beam displacement signal, defined by the amplitude of the position modulation. A simple case of the dipole moment spectrum of a single bunch in a ring accelerator, observed by a BPM can be estimated to [3]:

$$Z(\omega) I_{beam}(\omega) = D(\omega) = \\ = \omega_{rev} A_0 \sum_{n=-\infty}^{+\infty} \delta[\omega - (n\omega_{rev} + \omega_\beta)] e^{-\frac{(\omega - \omega_\beta - \omega_\xi)^2 \sigma_\tau^2}{2}} \quad (3)$$

and provides much more relevant information of accelerator and beam quality than just the static orbit.

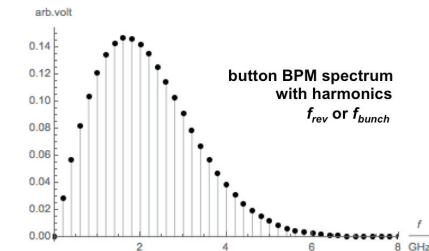


Figure 7: Button electrode spectrum for periodic bunches.

Figure 7 shows the same button electrode signal spectrum, now in linear scaling of the magnitude, and

sampled with f_{rev} or f_{bunch} , as of the periodic repetition of the bunched beam. In practice the signal spectrum may be more complex. The beam formatting often produces batches of bunches with gaps, bunches of different intensities, etc. The accelerator has non-linearities that lead to coupled oscillations, and the oscillation amplitude of each particle in a bunch, as well as of each bunch may be different.

Resonant BPM Pickups

A cylindrical resonator of radius R and length l has eigenmodes at frequencies:

$$f_{mnp} = \frac{1}{2\pi\sqrt{\mu_0\varepsilon_0}} \sqrt{\left(\frac{j_{mn}}{R}\right)^2 + \left(\frac{p\pi}{l}\right)^2} \quad (4)$$

and with added beam pipe ports, can be operated as beam excited, passive cavity BPM. The beam couples to the longitudinal components of the E-field of the eigenmodes, for dimensions $l < 2R$ the TM_{010} is the fundamental monopole mode, sensitive to the beam intensity, while the TM_{110} lowest dipole mode is proportional to beam displacement and intensity.

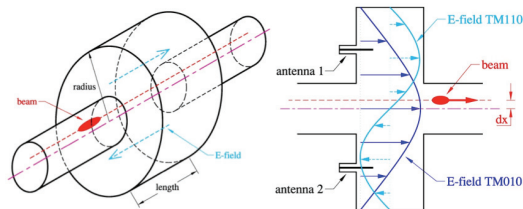


Figure 8: Beam excited, passive cylindrical resonator operating as cavity BPM.

Figure 8 illustrates the principle of operation. A simple pin antenna is used to detect the signal, however, to benefit from the high resolution potential of this BPM type a more sophisticated signal coupling schema needs to be implemented.

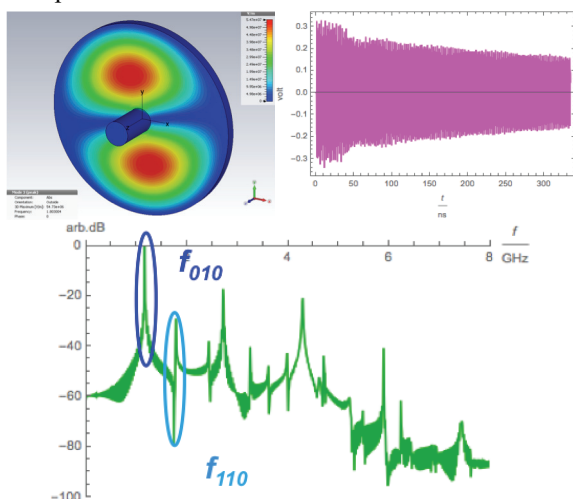


Figure 9: Cavity BPM signals.

Using the same bunch properties as for the broadband BPM examples, Fig. 9 shows the dipole mode of a

simplistic cavity BPM resonator of dimensions $R = 100$ mm, $l = 10$ mm, and the resulting time domain output signal for the $y = +1$ mm displaced beam (upper trace). For computation time reasons, the simulation was truncated at 350 nsec, therefore the corresponding frequency spectrum (lower plot) shows some artefacts. However, the important modes at $f_{010} \approx 1.15$ GHz and $f_{110} \approx 1.8$ GHz can be clearly identified.

As of the presence of many unwanted modal components in the output signal, the processing of the cavity BPM signals has substantially different objectives, compared to those of the broadband BPMs. For the cavity BPMs, analog RF and microwave electronics are necessary, the backend and DAQ technologies may nevertheless be quite similar to that of a button or stripline BPM, and based on digital signal processing.

Signal Processing Objectives

The processing of the BPM pickup signals has two main objectives

- **Normalization** Extract beam intensity independent displacement information, e.g. by relating difference and sum signal information from the BPM electrode pair. This can be accomplished by using analog RF techniques, e.g. Δ - Σ (180°) or 90° -hybrids, logarithmic amplifiers, etc. or by mathematical manipulation of the digitized signals of the individual electrodes.
- **Processing of broadband signals, decimation** The BPM pickup signals need to be conditioned for digitalization, which includes filters, gain stages and switchable attenuators, as well as analog down-conversion. In the digital domain the data needs to be further demodulated, decimated and filtered to the appropriate level, e.g. synchronized turn-by-turn position data, high resolution narrowband beam orbit data, etc.

To ensure stable BPM operation, the BPM electronics may include calibration or test signals, or switching elements to compensate drift effects of individual channels that otherwise would result in “electronic offsets”. The signal processing may also provide valuable beam intensity and/or beam phase (timing) information at each BPM station. Location and other design aspects of the BPM read-out electronics should minimize the cable length (expenses) between BPM pickup and electronics, which also will improve the performance.

BPM SIGNAL PROCESSING

Figure 10 shows the main building blocks of a typical BPM station. An analog signal conditioning section is required to adapt the signals for quantization at the ADC. Today, most of the BPM signal processing objectives can be accomplished in the digital domain (digital signal processing and data acquisition blocks). The question to answer is, how much analog technology is still required for the signal conditioning. The BPM block schematics

also indicate some of the necessary auxiliary elements, e.g. calibration section, clock-, timing-, and trigger signals, power supplies, etc.

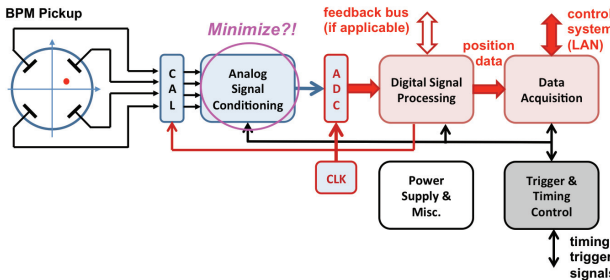


Figure 10: BPM building blocks.

Analog BPM Example: The Multiplexed Heterodyne Receiver

Let us define a BPM read-out system based on analog signal processing as electronics system, which utilizes all the normalization, demodulation, filtering and other signal gymnastics of the pickup signals before the digitalization. Now the requirements for the ADC, in terms of sampling rate, analog bandwidth and dynamic range are substantially reduced, on the costs of more complex analog and RF electronics. An overview of the various analog signal-processing schemas is given in [4].

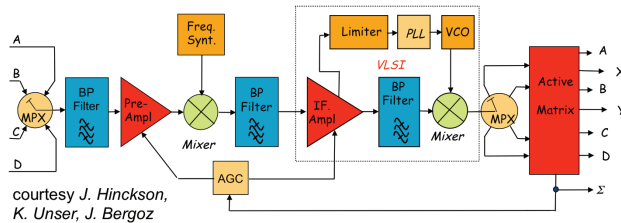


Figure 11: Analog heterodyne receiver based BPM electronics.

MPX Heterodyne Receiver A prominent example of BPM signal processing based on analog and RF electronics uses the heterodyne receiver concept, see Figure 11 [5]. It basically follows the classical radio receiver schema, the input signal is band-pass filtered, amplified and down-converted to an intermediate frequency (IF). The IF signal is further filtered, amplified, and finally detected by a synchronous demodulator. To scope with drift effects of analog components, the four BPM electrode signals are time multiplexed on a single receiver. An active matrix temporary stores the information and executes the normalization using operational amplifiers. The system operates with a narrow bandwidth and provides a high resolution ($\sim 1 \mu\text{m}$) beam orbit measurement, however, no turn-by-turn beam positions.

RF Mixer The analog RF mixer is a key element for downconversion and demodulation of RF signals. The ideal mixer multiplies the RF input signal

$$y_{RF}(t) = A_{RF} \sin(\omega_{RF} t + \varphi_{RF})$$

with the LO signal from a local oscillator

$$y_{LO}(t) = A_{LO} \sin(\omega_{LO} t + \varphi_{LO})$$

which results in upper and lower sideband signals at $f_{IF}=f_{RF} \pm f_{LO}$:

$$y_{IF}(t) = \frac{1}{2} A_{LO} A_{RF} \left\{ \sin[(\omega_{RF} - \omega_{LO})t + (\varphi_{RF} - \varphi_{LO})] + \sin[(\omega_{RF} + \omega_{LO})t + (\varphi_{RF} + \varphi_{LO})] \right\}$$

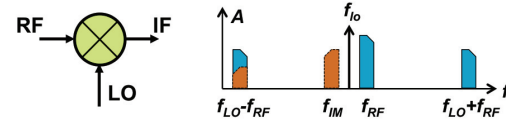


Figure 12: Analog RF mixer as downconverter.

For frequency conversion applications the mixer can be used as down-converter in a heterodyne receiver, typically $f_{RF} > f_{LO}$, or as demodulator or phase detector in homodyne operation with $f_{RF} = f_{LO}$. If no special care is taken, e.g. image rejection, the mixer will also down-convert the band at the image frequency, $f_{IM} = f_{LO} - f_{RF}$, which would be converted as indistinguishable alias to f_{IF} (see Figure 12). The “real” mixer is based on the non-linear characteristics of the Schottky diode,

$$I = I_0 (e^{V/V_T} - 1)$$

which results in additional mixing frequencies, giving $f_{IF} = m f_{RF} \pm n f_{LO}$. Particular care has to be taken to avoid unwanted mixing products appearing in the IF-band, e.g. filters, image rejection (SSB) mixing, etc.

BPMs Read-out Electronics Based on Analog and Digital Signal Processing Elements

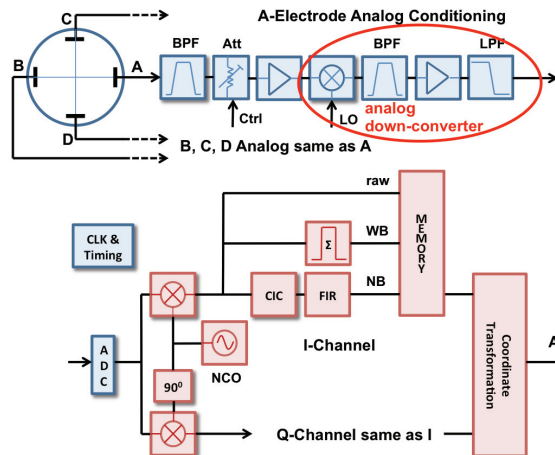


Figure 13: Schema of BPM read-out electronics, 1-out-of-4 channels shown.

Figure 13 shows the block diagram of a typical BPM read-out electronics for broadband BPM pickups, i.e. button or stripline monitors, heavily based on digital signal processing elements (only 1-out-of-4 channels is depicted). Often, the analog downconverter, highlighted in the analog signal conditioning section, is not required,

and a direct under-sampling to based-band demodulation is preferred.

The processing of the BPM signals in digital domain provides several advantages compared to analog schemes:

- Better reproducibility and stability of the beam position measurement, i.e. robust to environmental conditions (temperature, humidity, etc., however, not necessarily to radiation), no aging or drift effects, deterministic (no noise or statistical effects on the position information).
- Flexibility, i.e. modification of FPGA firmware, control registers or DAQ software allows to adapt the measurement to different beam conditions or operational requirements.
- Often the digital signals processing gives a better performance to the position measurement, e.g. higher resolution and stability, also because there is no analog equivalent to digital filters and data processing elements.

However, digital signal processing is not always better. The latency of the pipeline ADCs, quantization and clock jitter effects, as well as dynamic range and bandwidth limitations can degrade the performance substantially, or may limit the application. Also, to fully benefit from the digital technologies, the implementation often tends to be more complex than analog signal processing techniques, and require more manpower, costs and development time.

“Ringing” Bandpass Filter Even with state-of-the-art ADCs the time compressed BPM signals (Fig. 4) cannot be directly quantized with a sufficient dynamic range.

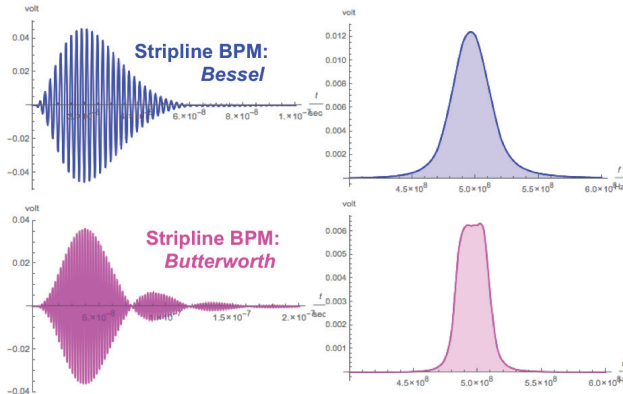


Figure 14: “Ringing” bandpass filter.

As the signal level reduces substantially because most energy of the input signal is rejected, a gain stage is switched into the signal path (Fig. 13), often in combination with a switchable RF attenuator to provide operational flexibility in terms of beam intensity range.

In case of multibunch operation, with a bunch spacing $t_{bunch} < t_{rise}$ of the filter rise time, a constructive signal pile-up effect has to be taken into account. Figure 15 shows the resulting signals for different bunch spacing's for our stripline BPM / Bessel filter example.

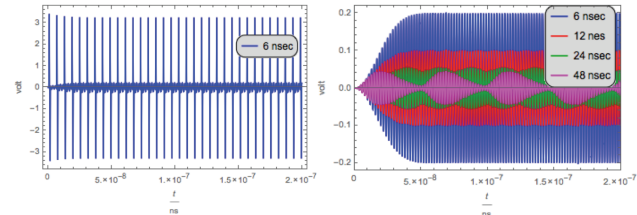


Figure 15: Multibunch signal pile-up effect, left: input signal ($t_{bunch}=6\text{ns}$), right: output signal for different bunch spacing's

Analog-Digital Converter (ADC) The ADC is the central element of the BPM signal processing, and has a major impact on the concept and overall performance of the BPM read-out system.

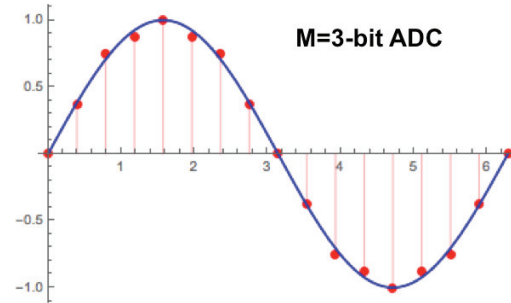


Figure 16: Quantization of a sinusoidal signal with a 3-bit ADC.

The ADC quantizes the continuous input signal waveform at equidistant spaced time samples. The digital output data is discrete in amplitude and time. The LSB voltage (resolution), $Q = V_{FSR}/2^M$ is given by the number of bits M and the full-scale range voltage V_{FSR} . Figure 16 shows the quantization effect for a 3-bit ADC on a sinusoidal signal. For $M=14$ or 16-bit, and $V_{FSR} = 1$ volt the LSB voltage is $Q = 61 \mu\text{V}$ (14-bit) or $15 \mu\text{V}$ (16-bit), demanding stable reference and supply voltages.

The maximum achievable dynamic range due to the quantization error is than given by

$$SNR = 20 \log_{10}(2^M) \quad (5)$$

which is 84 dB for 14-bit, and 96 dB for 16-bit ADCs.

However, in practice the dynamic range is limited due to the aperture jitter t_a of the clock signal, and degrades with higher frequency f of the input signal (see Fig. 17):

$$SNR = -20 \log_{10}(2\pi f t_a) \quad (6)$$

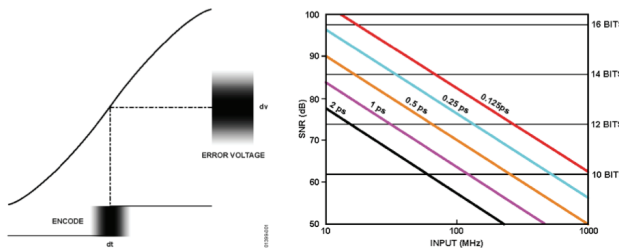


Figure 17: ADC SNR limit due to aperture (clock) jitter.

Following our example with a frequency $f \approx 500$ MHz of the input signal, and assuming an excellent low clock signal jitter of $t_a = 0.25$ ps, the dynamic range would be limited to $SNR = 62$ dB, equivalent to $EOB = 10.3$ (effective number of bits).

On the positive side, the BPM signal processing correlates the samples of 2 or 4 ADCs for the position data, by clocking them with the same signal. This correlates the aperture jitter, thus ensures reasonable small errors on the position measurement, even in presence of a rather large jitter of the clock signal.

Table 1: Performance of ADCs

Type	Res. bit	f_s MSPS	BW MHz	SNR@ f_{in} dB@MHz
AD9652	16	310	485	72@170
AD9680	14	1000	2000	67@170
LTM9013*	14	310	300*	62@150
ADC16DX..	16	370	800	69@150
ADS5474	14	400	1280	70@230

* has an analog I-Q mixer integrated, $0.7 < f_{in} < 4$ GHz

As of the time of writing (September 2014), there is a large variety of fast sampling ADC chips available. Table 1 summarizes a few examples of 14 and 16-bit ADCs, comparing a few performance parameters. All these ADCs follow the so-called “pipeline” architecture, a chain of T&Hs, ADCs and DACs converting the signal in a pipeline manner until the desired quantization resolution is reached. The pipeline ADC requires a constant clock frequency, and typically has a rather long latency until the digitized data reaches the output register. Often these ADCs have two or more channels on a single chip with very little cross talk, e.g. for direct I-Q sampling. Some chips include analog components, e.g. analog mixers, gain stages, filters, etc.

Sampling Theory A band-limited signal $x(t)$, $B=f_{max}$, can be fully reconstructed from the sampled amplitude values, if the sampling frequency $f_s \geq 2f_{max}$ (Nyquist-Shannon theorem, [6]). The reconstruction of $x(t)$ by $x_n=x(nT)$ is based on the sinc-function (with $T=1/f_s$):

$$x(t) = \sum_{n=-\infty}^{+\infty} x_n \frac{\sin \pi(2f_{max}t - n)}{\pi(2f_{max}t - n)} = \sum_{n=-\infty}^{+\infty} x_n \text{sinc} \frac{t - nT}{T} \quad (7)$$



Figure 18: Band-limited signal (left), and sampling of a sinusoidal signal (right).

As Fig. 18 (left) shows, f_{max} of the band-limited signal is the frequency, where the signal level practically reaches zero, it is not the frequency defined by the 3 dB bandwidth!

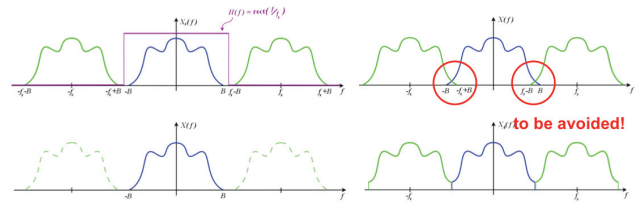


Figure 19: Aliasing effects.

The samples, e.g. of a sinusoidal signal of frequency f cannot be distinguished from an alias signal of same waveform, amplitude and phase, but twice the frequency, $2f$ (Fig. 18, right), in general: $f_{alias}(N)=|f-Nf_s|$. In the frequency domain this effect shows up as an image band (see Fig. 19, left). For the signal recovery based on eq. (7) a rectangular lowpass filter can be used to eliminate the unwanted image bands, however, if $f_s < 2f_{max}$ the bands overlap, and the reconstruction will fail (Fig. 19, right).

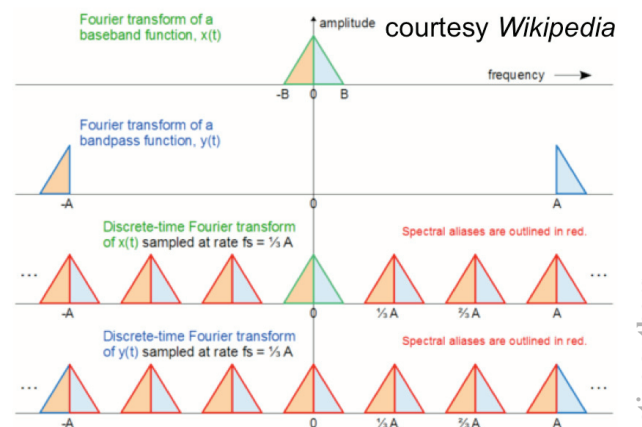


Figure 20: Bandpass or under-sampling.

A bandpass signal of $f_{hi}=A$ and $f_{lo}=A+B$ (see Fig. 20) can be down-converted to base-band (demodulated) if:

$$\frac{2f_{hi}}{n} \leq f_s \leq \frac{2f_{lo}}{n-1} \text{ with: } 1 \leq n \leq \left\lceil \frac{f_{hi}}{f_{hi}-f_{lo}} \right\rceil \quad (8)$$

Figure 20 illustrated the bandpass sampling for $f_s=f_{hi}/3$, showing the aliasing bands due to the undersampling. Figure 21 (left) demonstrates the undersampling concept on the single bunch Bessel filter response, with $T = 4$ ns, $f_s = 200$ MHz, $f_{hi}/f_{lo} = 550/450$ MHz, $n = 5.5$.

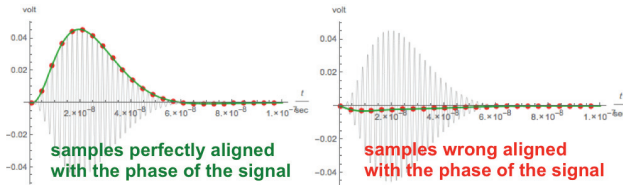


Figure 21: Undersampling of the 500 MHz Bessel filter single bunch response.

I-Q Sampling Figure 21 also demonstrates, the reconstruction requires the samples well aligned to the waveform, i.e. the phase between f_s and f_{in} . Applying the concept of I-Q sampling (see Fig. 22) on a sinusoidal waveform will avoid that problem [7]:

$$y(t) = A \sin(\omega t + \varphi_0)$$

$$y(t) = \underbrace{A \cos \varphi_0 \sin \omega t}_{=I} + \underbrace{A \sin \varphi_0 \cos \omega t}_{=Q} \quad (9)$$

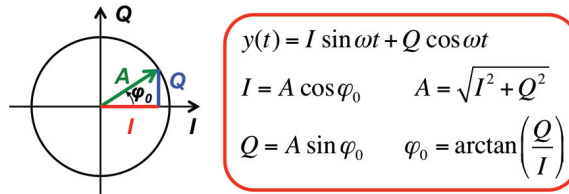


Figure 22: Concept of I-Q sampling.

The in-phase (I) and quadrature-phase (Q) components of the counter-clockwise rotating phasor of a sinusoidal frequency f are sampled with $f_s = 4f$. The signal amplitude A , as well as the phase φ_0 can be deduced independent of the relative phase (timing) between f_s and f . Figure 23 shows the principle (left), and the example on our 500 MHz Bessel filter response (right).

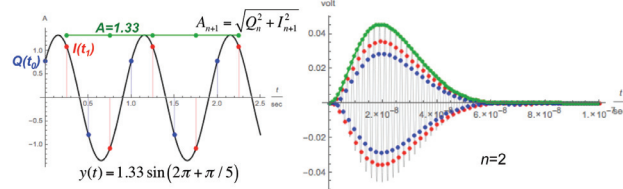


Figure 23: I-Q sampling of a sinusoidal signal (left), and of a 500 MHz Bessel filter response signal (right).

Direct Down-Converter (DDC) The I-Q sampling is applied in the digital down-converter (DDC), which converts the band-limited RF or IF signal to baseband (quadrature demodulation) and also serves for data reduction (filtering and decimation). Figure 24 shows the building blocks of a DDC [7]:

- A fast oversampling ADC
- A numerically controlled oscillator (NCO), based on a direct digital frequency synthesizer (DDS)
- Digital mixers (“ideal” multipliers)

- Decimation lowpass filters for anti-aliasing and data reduction, e.g. based on CIC and/or FIR filters.

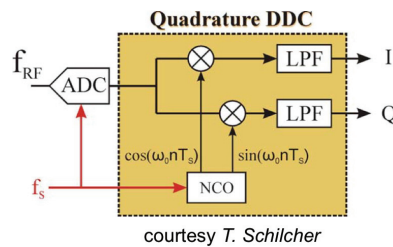


Figure 24: Building blocks of a digital down-converter.

Cascaded Integrator Com (CIC) Filter Because of the economical implementation, a decimating cascaded integrator comb filter (CIC) is often the preferred lowpass filter in the DDC implementation. It consists out of N integrators, a decimator R , and N comb filters (Fig. 25), forming a stable FIR filter with a sinc-function like transfer response [8]:

$$H(f) = \left(\frac{\sin \pi M \frac{f}{f_{out}}}{\sin \frac{\pi}{R} \frac{f}{f_{out}}} \right)^N \quad (10)$$

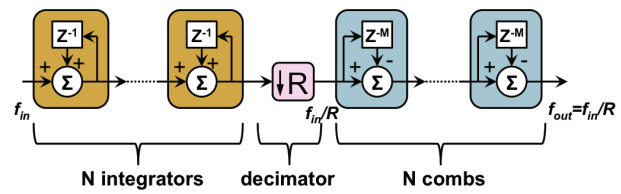


Figure 25: Cascaded integrator comb filter (CIC).

Figure 25 shows the architecture of the CIC filter. The output data rate (frequency) is decimated by $f_{out} = f_{in}/R$. Figure 26 (left) plots the frequency response of eq. (10). The differential delay M of the comb sections defines the location of the zeros, $f_0 = k f_{out}/M$. Care has to be taken on the aliasing / image bands of the CIC filter around: $(i-f_0) \leq f \leq (i+f_0)$, see Fig. 26 (right). Typically one or more FIR filters follow the CIC filter, one optimized to compensate the CIC passband drop.

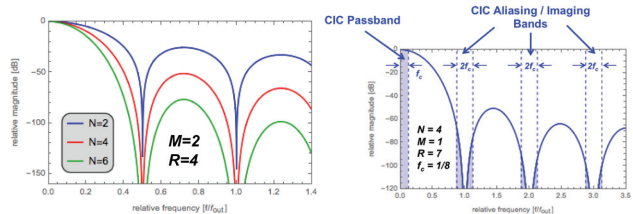


Figure 26: Cascaded integrator comb filter (CIC).

Signal/Noise (S/N) and BPM Resolution At the first gain stage (amplifier) of the analog signal conditioning (Fig. 13), the minimum noise voltage is expected to be:

$$v_{noise} = \sqrt{4k_B T R \Delta f} \quad (11)$$

For the single bunch example of the stripline BPM / *Bessel* bandpass, with $R = 50 \Omega$, $\Delta f = 25 \text{ MHz}$, $T = 300 \text{ K}$ the theoretical noise voltage computes $v_{noise} = 4.55 \mu\text{V}$ (-93.83 dBm). The signal-to-noise ratio is $S/N = \Delta v/v_{noise}$, with Δv being the BPM voltage signal at the amplifier input, reflecting a signal change due to the change of the beam position ($\Delta x, \Delta y$). At $f = 500 \text{ MHz}$, the signal level for our example is $v \approx 22.3 \text{ mV}$ (-20 dBm). This results in a $S/N \approx 4900$ (73.8 dB), which would be the required dynamic range to resolve the theoretical resolution limit of the BPM. Using the sensitivity of $\sim 2.7 \text{ mm}/\text{dB}$ of the stripline BPM, this corresponds to $\Delta x = \Delta y \approx 0.66 \mu\text{m}$.

In practice there are several factors that will reduce this theoretical S/N limit, e.g. insertion losses between BPM pickup and amplifier (cables, connectors, bandpass filter, couplers, etc.) and the noise figure of the 1st amplifier. Also, a useable S/N needs to be $> 0 \text{ dB}$. As a result the practically achievable S/N for this signal bunch signal is $\sim 10 \text{ dB}$ lower, and the corresponding resolution will be in the $2 \dots 3 \mu\text{m}$ regime.

Several factors can still improve the BPM resolution:

- Increase the signal level, e.g. by modifications of the pickup (larger electrodes, smaller beam pipe aperture), higher beam intensity.
- Increase the measurement (integration) time, and/or apply statistics on periodic signals or data, e.g. reduce the filter bandwidth in analog and/or digital sections ($S/N \sim 1/\sqrt{BW}$), apply data filtering by averaging ($S/N \sim \sqrt{n}$).

ANALOG VS. DIGITAL DOWN-CONVERSION

Processing the BPM electrode signals individually requires a large dynamic range. Linearity is the most important system aspect. Present ADC technologies are limited to $\sim 70 \text{ dB}$ of linear dynamic range, this is not sufficient for most BPM applications. At minimum, a set of gain stages and switchable attenuators has to be foreseen to extend to the necessary dynamic range, also a slow automatic gain control (AGC) feedback is an option.

An analog heterodyne down-converter for each channel, in front of the ADC (Fig. 13), will complicate the RF signal engineering, but offers also some advantages, e.g. allows the sampling in the 1st Nyquist passband (no undersampling), relaxes RF input filter requirements, relaxes ADC and clock signal requirements, and may even relax some cables requirements in case the analog RF hardware can be installed near the beam pickups (transfer the IF signals via long cables). Beside additional analog and RF hardware, we also may suffer from additional aliasing effects due to the frequency mixing, which count against this solution.

What is better? To some extend it is a matter of taste and engineering preference, but sure requires a very detailed analysis for the specific case to answer this question. For beam pickups operating at microwave frequencies, e.g. cavity BPM, a RF heterodyne receiver

stage in front of the digital electronics certainly is still necessary.

BPM PERFORMANCE

Applying and optimizing the discussed BPM signal-processing principles may lead to excellent performance of BPM systems. Depending of the specific case and the BPM requirements, better-tailored and advanced techniques should be followed, particular in the digital sections.

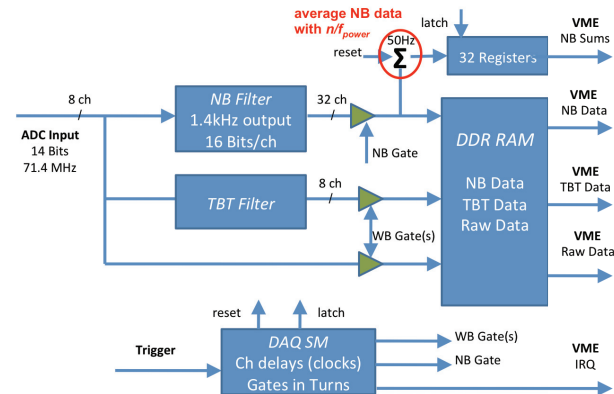


Figure 27: Digital signal processing for the ATF BPMs.

Figure 27 highlights the averaging feature of narrowband position data in multiples of the power-grid frequency, implemented at the digital signal processing for the ATF damping ring BPMs. This ensures clean, high-resolution beam position measurements, independent from the integration timing to the power grid frequency. Turn-by-turn and narrowband beam studies verified the ATF BPM performance, validating the measured optics functions (β -function, beating and phase advance) with the accelerator optics models [9].

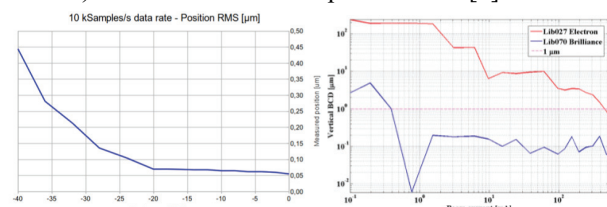


Figure 28: BPM performance *Libera Brilliance* +.

Figure 28 shows the performance of the *Libera Brilliance* + (*Instrumentation Technologies*) BPM system, at higher input signal levels the position resolution in narrowband (0.01...1 kHz) mode is $< 50 \text{ nm}$ (left), and the measured beam position is independent over a three decades of beam intensity (right). Applying a crossbar switch technique to eliminate drift and aging effects in the analog sections of the Libera BPM electronics, a $< 100 \text{ nm}$ stability over 14 hours could be demonstrated [10].

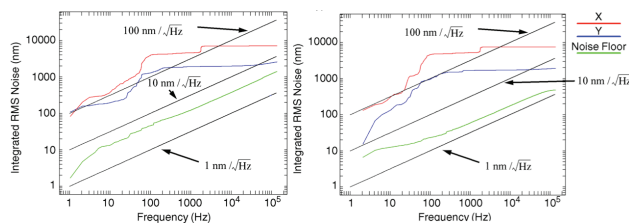


Figure 29: S/N performance of “home-brew” vs. commercial digital BPM electronics.

Figure 29 compares the performance of “home-brew” digital BPM read-out electronics to an earlier version of the commercial Libera system, noise floor and resolution performance show quite similar behaviour [11].

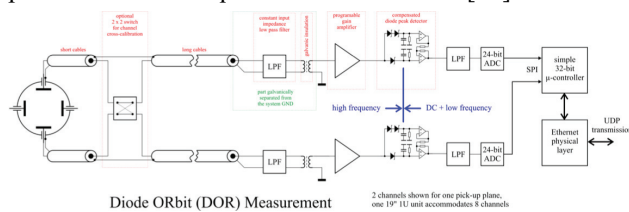


Figure 30: Beam orbit measurement based on diode detectors.

Advanced, and to some extend complex digital signal processing techniques demonstrated very high resolution and stability, however, pure analog BPM signal processing with minimalistic circuits can achieve similar results [12]. Figure 30 shows the schematics of beam orbit electronics based on a compensated diode detector, which demonstrated a resolution of <20

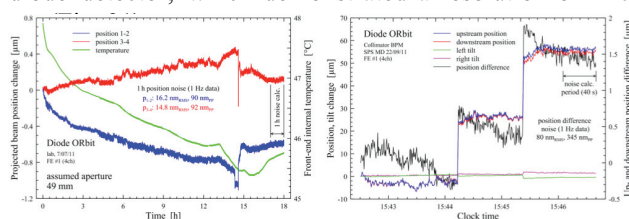


Figure 31: Performance of analog beam orbit read-out electronics based on compensated diode detectors.

REFERENCES

- [1] E. Calvo Giraldo, et al., “The LHC Beam Position System: Performance during 2010 and Outlook for 2011”, Proc. of DIPAC 2011, Hamburg, Germany, 2011, pp.323-325; <http://www.JACoW.org>
- [2] M. Wendt, “Overview of Recent Trends and Developments for BPM Systems”, Proc. of DIPAC 2011, Hamburg, Germany, 2011, pp.18-22; <http://www.JACoW.org>
- [3] R. H. Siemann, “Spectral Analysis of Relativistic Bunched Beams”, Proc. of BIW 1996, Argonne, IL, U.S.A., 1996, pp.3-22
- [4] G. Vismara, “Signal Processing for Beam Position Monitors”, Proc. of BIW 2000, Cambridge, MA, U.S.A., 2000, pp.36-60
- [5] J. A. Hinkson, K. H. Unser “Precision Analog Signal Processor for Beam Position Measurements in Electron Storage Rings”, Proc. of DIPAC 1995, Travemünde, Germany, 1995
- [6] Wikipedia, “Nyquist-Shannon Sampling Theorem”, http://en.wikipedia.org/wiki/Nyquist-Shannon_sampling_theorem
- [7] T. Schilcher, “Digital Signal Processing for RF Applications”, Digital Signal Processing CAS 2007, Sigtuna, Sweden, 2007, pp.249-283
- [8] E. B. Hogenauer, “An Economical Class of Digital Filters for Decimation and Interpolation”, IEEE Trans. on Acoustics, Speech and Signal Processing, vol. ASSP-29, No. 2, April 1981, pp.155-162
- [9] Y. Renier, et al., “Turn-by-Turn BPM Data Analysis from the ATF Damping Ring”, CLIC Workshop 2013, Geneva, Switzerland, 2013
- [10] P. Leban, *Instrumentation Technologies*, private communications
- [11] G. Decker, “Beam Position Monitors: How to Meet the Specifications of the Most Recent Accelerators”, Proc. of IBIC 2013, Oxford, UK, 2013, pp.623-629; <http://www.JACoW.org>
- [12] M. Gasior, et al., “BPM Electronics based on Compensated Diode Detectors – Results from Recent Development Systems”, Proc. of BIW 2012, Newport News, VA, U.S.A., 2012, pp.44-46; <http://www.JACoW.org>